World Academy of Science, Engineering and Technology
International Journal of Biomedical and Biological Engineering
Vol:8, No:11, 2014

Altered Network Organization in Mild Alzheimer's Disease Compared to Mild Cognitive Impairment Using Resting-State EEG

Chia-Feng Lu, Yuh-Jen Wang, Shin Teng, Yu-Te Wu, Sui-Hing Yan

Open Science Index, Biomedical and Biological Engineering Vol:8, No:11, 2014 publications.waset.org/9999740/pdf

***Abstract*—**Brain functional networks based on resting-state EEG data were compared between patients with mild Alzheimer's disease (mAD) and matched patients with amnestic subtype of mild cognitive impairment (aMCI). We integrated the time–frequency cross mutual information (TFCMI) method to estimate the EEG functional connectivity between cortical regions and the network analysis based on graph theory to further investigate the alterations of functional networks in mAD compared with aMCI group. We aimed at investigating the changes of network integrity, local clustering, information processing efficiency, and fault tolerance in mAD brain networks for different frequency bands based on several topological properties, including degree, strength, clustering coefficient, shortest path length, and efficiency. Results showed that the disruptions of network integrity and reductions of network efficiency in mAD characterized by lower degree, decreased clustering coefficient, higher shortest path length, and reduced global and local efficiencies in the delta, theta, beta2, and gamma bands were evident. The significant changes in network organization can be used in assisting discrimination of mAD from aMCI in clinical.

***Keywords*—**EEG, functional connectivity, graph theory, TFCMI.

I. Introduction

ALZHEIMER'S DISEASE (AD) is one of the most common neurodegenerative diseases. Patients with AD exhibit impairments in multiple cognitive domains, such as memory, executive functions, attention, visuospatial skill, and verbal ability. On the other hand, mild cognitive impairment (MCI) was regarded as an intermediate state of cognitive function between normal aging and AD [1]. Previous studies reported that MCI, especially amnestic subtype MCI (aMCI), may convert to AD at about 30-50% within 3-5 years [2], [3]. Therefore, early diagnosis of MCI and discrimination from mild AD (mAD) can be helpful to improve disease progression following therapeutical interventions.

Previous studies reported that AD and aMCI were not only associated with regional alterations in brain activity, but also with abnormal functional integration between different brain regions, suggesting AD or aMCI as a disconnection syndrome [4], [5]. Therefore, functional connectivity analysis can be used to provide the discriminative features for investigating the differences between mAD and aMCI.

Functional connectivity can be measured by estimating synchrony of the electroencephography (EEG) signal oscillations between cortical regions. EEG oscillations are generated locally in different brain regions and mediate coordinated interactions within and between different neural systems to form functional networks. Many researchers have used coherence analysis to measure cortical functional connections. However, the coherence method only measures linear dependency between neural signals and may be insufficient for studying complex and nonlinear brain dynamics [6]. The coherence method can be problematic if the signals are contaminated by noise or the oscillatory frequency band is not carefully defined [7], [8]. The time–frequency cross mutual information (TFCMI) method offers an alternative solution [9], which calculates the mutual information between two temporal power sequences within a specific band, and serves as a statistical measure of linear and nonlinear dependencies between cortical regions [10].

Recent neurophysiological and neuroimaging studies have used advanced graph theoretical network analysis approaches to demonstrate that AD patients have disruptive neuronal integrity in large-scale structural and functional brain systems during cognitive tasks and at resting-state [11], [12]. Studies on functional network derived from EEG and functional magnetic resonance imaging also reported that AD patients presented sparser and less efficient organization of functional networks compared with healthy controls [11], [12].

In the present study, we integrated the TFCMI method to estimate the EEG functional connectivity between cortical regions and the network analysis based on graph theory to further investigate the difference of functional networks between aMCI and mAD groups in their global and local topological properties, including degree, strength, clustering coefficient, shortest path length, and efficiency, for six different frequency bands.

C. F. Lu and Y. J. Wang contributed equally to this article.

C. F. Lu is with the Image Research Center, College of Medicine, Taipei Medical University, Taipei, Taiwan; Department of Physical Therapy and Assistive Technology, National Yang-Ming University, Taipei, Taiwan; and with the Department of Education and Research, Taipei City Hospital, Taipei, Taiwan (e-mail: alvin4016@yahoo.com.tw).

Y. J. Wang is with the Department of Neurology, Taipei City Hospital, Ren-Ai Branch, Taipei, Taiwan (e-mail: DAL29@tpech.gov.tw).

S. Teng is with the Department of Biomedical Imaging and Radiological Sciences, National Yang-Ming University, Taipei, Taiwan (e-mail: iamtengshin@yahoo.com.tw).

Y. T. Wu is with the Institute of Biophotonics, National Yang-Ming University, Taipei, Taiwan (e-mail:ytwu@ym.edu.tw).

S. H. Yan is with the Department of Neurology, Taipei City Hospital, Ren-Ai Branch, Taipei, Taiwan (corresponding author, phone: +886-2-2709-3600 ext.3711; fax: +886-2-2704-6356; e-mail: DAK02@ tpech.gov.tw).

Open Science Index, Biomedical and Biological Engineering Vol:8, No:11, 2014 publications.waset.org/9999740/pdf

II. Materials and Methods

A. Participants

This study received prior approval from the Institutional Review Board of Taipei City Hospital. We retrospectively enrolled aMCI and mAD patients with EEG examinations. Each subject first visit the Department of Neurology in Taipei City Hospital during 2007–2011. Their clinical data regarding dementia and cognitive decline were collected, including clinical histories, neurological examinations, neuroimaging studies (CT or MRI), neuropsychological interview, mini-mental state examination (MMSE) [13], and clinical dementia rating (CDR) [14]. All recorded clinical data was reviewed to exclude participants with (1) evidence of other neurological or psychiatric diseases characterized by the cognitive impairment; (2) uncontrolled or complicated systemic diseases or traumatic brain injuries; and (3) the mixed dementia that can lead to atypical AD symptoms.

The diagnosis of aMCI met the Petersen criteria [15]. The inclusion criteria for aMCI participants in this study were: (1) CDR score of 0.5; (2) MMSE score of 20–25; and (3) memory decline in the absence of dementia or significant functional loss. AD was diagnosed according to NINCDS-ADRDA criteria for "probable AD" [16]. The inclusion criteria for mAD were (1) CDR score of 1; and (2) MMSE score less than 25.

Finally, the clinical data and EEG of 24 aMCI and 13 mAD were enrolled in this study for the subsequent analysis. Table I summarizes the demographic features and clinical data of study groups. No significant age and gender differences were observed between the aMCI and mAD groups.

B. EEG Recordings and Preprocessing

The EEG data during resting state were recorded from 19 scalp electrodes using a Nihon-Kohden EEG-1000 system (Nihon-Kohden Inc., Tokyo, Japan) at a sampling rate of 200 Hz and impedance of less than 7 kΩ at each electrode. The 19 electrodes were positioned according to the international 10–20 system including Fp1, Fp2, F3, F4, C3, C4, P3, P4, O1, O2, F7, F8, T3, T4, T5, T6, Fz, Cz, and Pz. All the EEG activities were referenced to the average signal of the two linked mastoid electrodes and bandpass filtered between 1 and 40 Hz. Both eyes-closed and eyes-opened conditions were recorded for 20–30 s alternately to a total of 4 minutes for each condition. Subjects remained awake and alert during the recording without increased attentional demand or cognitive load. Only the eyes-closed EEG data were extracted and segmented into approximate 110 consecutive epochs of 2 s in the present study.

To eliminate the ocular, muscular, and other types of physiological artifacts, we first reviewed each epoch and manually discarded the bad epochs with aberrant waveforms or large signal drifts. The averaged rejection rates of epochs are $24.90 \pm 9.94\%$ for aMCI and $24.43 \pm 10.87\%$ for mAD group. Second, the algorithm of independent component analysis was utilized to decompose the EEG signals into multiple independent components, allowing artifacts to be easily detected and rejected [17]. The rejection criteria of independent components were that: (1) the scalp voltage map presents a far-frontal projection which is a typical artifact of eye movement; (2) the map is marginally localized with high-frequency powers; or (3) the component activities originated from few specific epochs and did not consistently distribute across epochs. The number of rejected components are $3.38 \pm 1.69\%$ for aMCI and $3.06 \pm 1.29\%$ for mAD group.

Finally, approximate 80 artifact-free epochs for each participant were used for further analysis.

TABLE I
Demographic Features and Clinical Data of Study Groups

	aMCI (n = 24)	mAD (n = 13)	*P* value
Age[a]	81.13 ± 3.95	82.62 ± 4.81	0.32
Sex[b](male/female)	6/18	3/10	0.79
MMSE	20.79 ± 4.80	14.31 ± 5.01	0.0004
CDR	0.5	1.0	

[a]Continuous data are expressed as mean ± standard deviation and were tested by the Kruskal–Wallis test.
[b]Sex data were tested by the Pearson chi-square test.
MMSE, mini-mental state examination; CDR, clinical dementia rating.

C. Source Signal Estimation

In this study, the signals of cortical source were estimated from the scalp EEG data by two steps, namely, the forward model followed by an inverse operation. The forward head model was constructed based on a symmetric boundary element using OpenMEEG package (http://openmeeg.github.io/) [18]. To compute the inverse operator, minimum-norm estimation (MNE) with depth-weighting approach was used to obtain the source signals along the entire cortical surface of the EEG data [19]. The specific parameters are given as follows: (a) the source orientations were set to be unconstrained on the cortical surface; (b) a depth weighting algorithm was used to compensate for the biased calculations of superficial sources [20]; and (c) a regularization parameter, $\lambda^2 = 0.1$, was used to reduce numerical instability of the MNE and obtain a spatially smoothed solution [7]. The MNE analysis was performed using Brainstorm software (http://neuroimage.usc.edu/brainstorm) [21].

Cortical surface maps of source activity in each subject were displayed on the standard Colin27 anatomical images in Montreal Neurological Institute (MNI) space [22]. We further extracted the time-varying current strengths in 62 cortical surface regions covering entire cerebral cortex for each epoch based on a Mindboggle atlas (Table II) [23].

D. Brain Network Construction

The functional brain network for each participant was represented by a 62×62 graph consisting of 62 nodes (cortical regions) and edges (functional connectivity between regions). The functional connectivity between cortical surface regions was measured using the time-frequency cross mutual information (TFCMI) analysis, which is more resistant to reference selection and noise interference than the coherence method [9], [24].

Open Science Index, Biomedical and Biological Engineering Vol:8, No:11, 2014 publications.waset.org/9999740/pdf

TABLE II
CORTICAL SURFACE REGIONS AND THEIR ABBREVIATIONS (ALL FOR BOTH HEMISPHERES)

Type	Name	Label	Type	Name	Label
PF	Medial orbitofrontal	MOF	PF	Lateral orbitofrontal	LOF
PF	Parsorbitalis	PO	F	Superior frontal	SF
F	Caudal middle frontal	CMF	F	Rostral middle frontal	RMF
F	Parsopercularis	POP	F	Parstrangularis	PT
C	Paracentral	paraC	C	Precentral	preC
C	Postcentral	postC	P	Precuneus	precun
P	Surperior parietal	SP	P	Inferior parietal	IP
P	Supramarginal	SM	T	Superior temporal	ST
T	Middle temporal	MT	T	Inferior temporal	IT
T	Transverse temporal	TT	T	Insula	insula
T	Parahippocampus	paraH	T	Entrohinal	EC
T	Fusiform	fusiform	L	Rostral anterior cingulate	RAC
L	Caudal anterior cingulate	CAC	L	Posterior cingulate	PC
L	Isthmus cingulate	IC	O	Cuneus	cuneus
O	Lingual	lingual	O	Pericalcarine	periCal
O	Lateral occipital	LO			

PF, prefrontal; F, frontal; C, central; P, parietal; T, temporal; L, limbic; O, occipital.

The TFCMI analysis consists of two processing steps, i.e. the wavelet transformation and mutual information calculation. First, the surface source signal in each region and each epoch was transformed into the time-frequency domain using the Morlet wavelet transformation to obtain temporal spectral map (Fig. 1 (b)) [9]. The frequency resolution was 1 Hz and temporal resolution was 5 ms. Six sets of time-frequency maps encompassing the *delta* (1-4 Hz), *theta* (5-7 Hz), *alpha* (8-12 Hz), *beta1* (13-20 Hz), *beta2* (21-30 Hz), and *gamma* (31-40 Hz) activities were created separately. The power across selected frequency bands in each cortical region was averaged to produce a dynamic power curve (Fig. 1 (c)). The temporal series of averaged power signals were then used to compute the cross mutual information (CMI) between any two cortical regions in each epoch [9]. Denote the averaged power signals at the *i*th region by a random variable, F_i, and its probability density function (PDF) by $p(F_i)$.

$$CMI_{i,j} = \sum_{b=1}^{40} p(F_{i,b}, F_{j,b}) \ln\left(p(F_{i,b}, F_{j,b}) / p(F_{i,b}) p(F_{j,b})\right) \quad (1)$$

where b=1,2,…,40 represents the index of sampling bins used to construct the approximated PDF and joint PDF. Finally, the functional connections in each epoch and each frequency band were generated by a pair of regions, creating a 62×62 TFCMI map (Fig. 1 (d)). The TFCMI values were normalized so that the maximal values equal one. A schematic diagram for the construction of a functional network is shown in Fig. 1.

E. Network Analysis

The 62×62 TFCMI maps for each selected frequency band were first binarized by applying threshold T to the weighted edges.

$$e_{ij} = \begin{cases} 1, & \text{if } CMI_{i,j} \geq T \\ 0, & \text{otherwise} \end{cases} \quad (2)$$

where e_{ij} is referred to as the effective connection between cortical regions *i* and *j*. We set thresholds *T* equal to the mean value of whole TFCMI map added by one standard deviation for all participants. The threshold for each selected band in this study was 0.52 in delta, 0.41 in theta, 0.34 in alpha, 0.27 in beta1, 0.21 in beta2, and 0.18 in gamma, respectively.

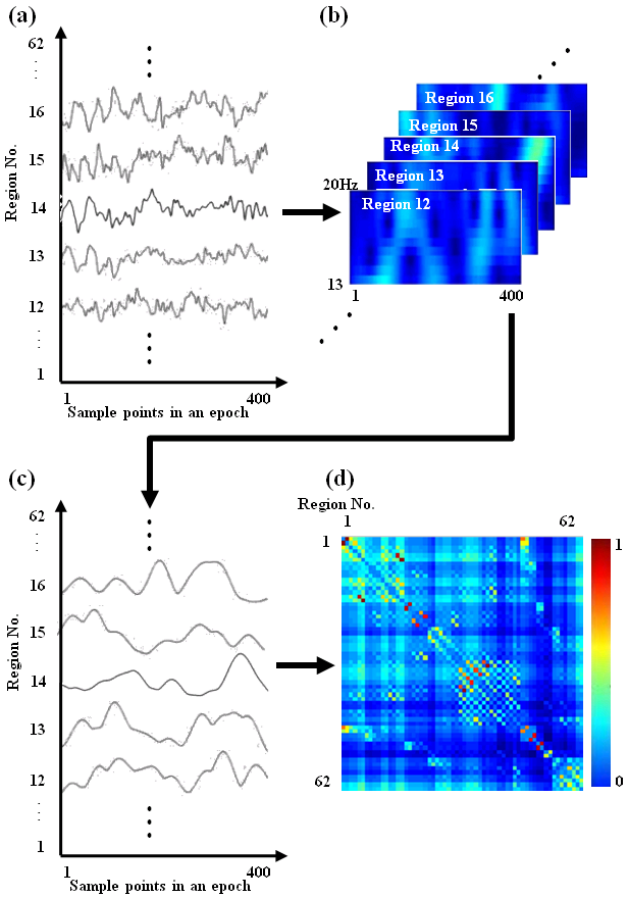


Fig. 1 Schematic diagram of the functional network construction. (a) The EEG source signals for 62 cortical surface regions of each epoch. (b) The source signal were processed using the Morlet wavelet transformation to obtain time–frequency power maps within the selected frequency band (beta1, 13–20 Hz shown here), in which colors indicate power amplitude in an arbitrary unit (a. u.). (c) The averaged power signal for each region was created by averaging the individual time–frequency maps across selected frequency band. (d) The 62×62 TFCMI map was obtained by calculating the cross mutual information from the averaged powers between any two channels

Network organization can be estimated by topological properties based on graph theory. Five regional properties, including nodal degree (k_i), nodal strength (s_i), nodal clustering coefficient (c_i), nodal shortest path length (l_i), and nodal efficiency ($E_{nodal}(i)$), were computed for each node. The nodal degree is the number of functionally connected neighbors to a node; the nodal strength represents the functional synchrony

Open Science Index, Biomedical and Biological Engineering Vol:8, No:11, 2014 publications.waset.org/9999740/pdf

with other nodes for a node; the nodal clustering coefficient is the probability of interconnectivity between neighboring nodes in a network; the nodal shortest path length represents the separation between any pair of nodes in a network; the nodal efficiency quantifies the importance of a node for communication within the network [25]-[29]. The topological properties were calculated as follows:

$$k_i = \sum_{j \in N} e_{ij} \tag{3}$$

$$s_i = \frac{1}{k_i} \sum_{j \in N} CMI_{ij} \cdot e_{ij} \tag{4}$$

$$c_i = \left(1 / k_i \left(k_i - 1\right)\right) \sum_{j,h \in N} e_{ij} e_{ih} e_{jh} \tag{5}$$

$$l_i = \frac{1}{n-1} \sum_{j \in N, j \neq i} d_{ij} \tag{6}$$

$$E_{nodal}(i) = \frac{1}{n-1} \sum_{j \in N, j \neq i} d_{ij}^{-1} \tag{7}$$

where n is the number of nodes, N is the set of full brain network, and d_{ij} is the minimal number of edges that must be traversed to form a connection between nodes i and j.

Six global properties, degree (K), strength (S), clustering coefficient (C), shortest path length (L), global efficiency (E_{global}), and local efficiency (E_{local}), were used to evaluate whole-network structure [26], [27]. The global efficiency of a network represents the ability of transmitting and processing parallel information in a network. All global properties are calculated as:

$$K = \frac{1}{n} \sum_{i \in N} k_i \tag{8}$$

$$S = \frac{1}{n} \sum_{i \in N} S_i \tag{9}$$

$$C = \frac{1}{n} \sum_{i \in N} c_i \tag{10}$$

$$L = \frac{1}{n} \sum_{i \in N} l_i \tag{11}$$

$$E_{global}(N) = \frac{1}{n} \sum_{i \in N} E_{nodal}(i) \tag{12}$$

$$E_{local}(N) = \frac{1}{n} \sum_{i \in N} E_{global}(N_i) \tag{13}$$

where the subgraph N_i is a set, consisting of the direct neighboring nodes of node i. Note that the node i is not an element of subgraph N_i. Therefore, the local efficiency can be considered to be a measure of the fault tolerance for a network; that is, how well the information can be exchanged within each subgraph when the index node is eliminated.

F. Statistics

Global properties were separately examined by two-sample t test to decide whether the means of these measurements were significantly different ($p < 0.05$) between aMCI and mAD groups for each selected frequency band. The nodal (regional) properties were separately examined region-by-region using two-sample t test to investigate the significant difference ($p < 0.05$) between aMCI and mAD groups. For the statistics in nodal properties, the p values were corrected using the false discovery rate (FDR) method for multiple comparisons across 62 cortical regions [30].

III. Results and Discussions

A. Global Network Properties

The 6 global network properties in each selected frequency band for aMCI and mAD groups are displayed in Fig. 2. Results showed that the brain functional networks in mAD exhibited altered network architecture involving the delta, theta, beta2, and gamma bands compared with that in aMCI. Generally, the functional networks in mAD were sparser (lower degree and clustering coefficient in Figs. 2 (a) and (c), less efficient in information transmission (higher shortest path length in Fig. 2 (d) and lower global efficiency in Fig. 2 (e) and), and with lower tolerance to resist abnormalities (lower local efficiency in Fig. 2 (f)) than brain networks in aMCI. The declines in global network properties supported the previous findings that AD exhibited disrupted distant brain functional connectivity and therefore reduce the integrity of whole-brain network [31], [32].

B. Nodal Network Properties

The results of significant differences ($p < 0.05$ with FDR correction) in nodal network properties between mAD and aMCI groups are separately displayed in Figs. 3-6. Due to the space limitation, only the frequency bands with significant differences in nodal properties were depicted.

Bilateral medial orbitofrontal cortices (MOF) exhibited significant increases in nodal strength in the theta and delta bands for mAD (Figs. 3 (a) and (b)). Theta-frequency activity, which arises from the hippocampus and oscillates with medial frontal and cingulate cortex, is associated with memory functions [33], [34]. This result suggested that the mAD patients have stronger functional connectivity related to the bilateral medial orbitofrontal regions in the low-frequency fluctuations, which may be compensation to the disruption to the hippocampus-related connectivity. In contrast, the right parahippocampus exhibited significantly reduced nodal strength in the delta band for mAD (Fig. 3 (a)). The decline of the nodal strength in parahippocampus gyrus may suggest the impairment of memory encoding and retrieval in mAD patients.

Open Science Index, Biomedical and Biological Engineering Vol:8, No:11, 2014 publications.waset.org/9999740/pdf

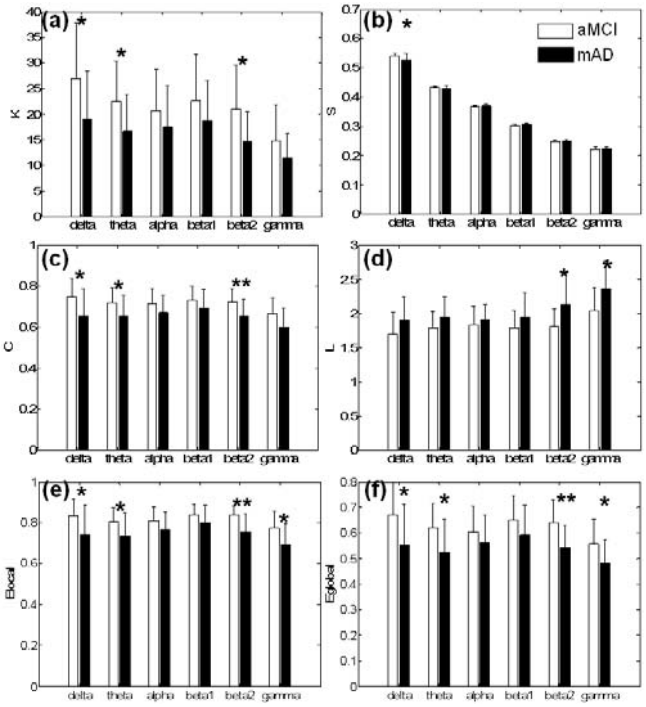


Fig. 2 The global network properties, (a) degree, (b) strength, (c) clustering coefficient, (d) shortest path length, (e) global efficiency, and (f) local efficiency, in each frequency band for aMCI and mAD groups. *, $p < 0.05$; **, $p < 0.005$

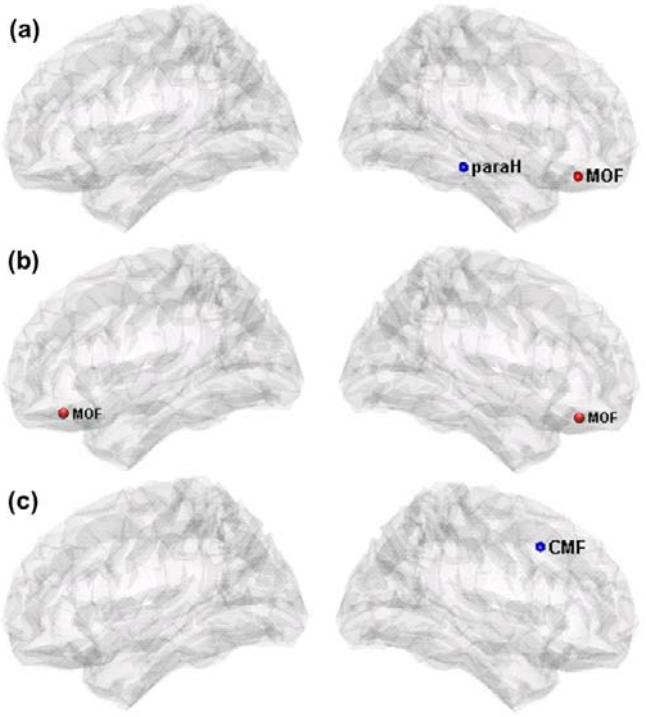


Fig. 3 The cortical regions with significant changes in nodal strength for mAD compared with aMCI in the (a) delta, (b) theta, and (c) gamma bands. The plots are displayed from left (left column) and right (right column) lateral views

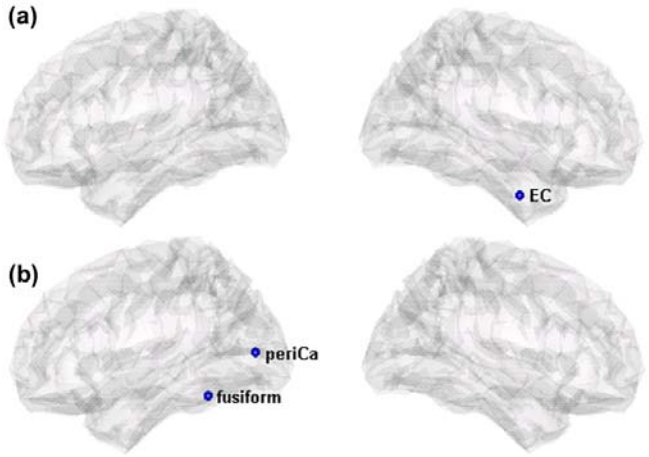


Fig. 4 The cortical regions with significant decreases in nodal clustering coefficient for mAD compared with aMCI in the (a) delta and (b) beta2 bands. The plots are displayed from left (left column) and right (right column) lateral views

Significant increases in nodal shortest path length for mAD were found in several central regions (preC and postC), right middle frontal (CMF), and right inferior frontal regions (PT and PO) in addition to the bilateral parietal and occipital regions in the higher frequency bands, namely, the beta2 and gamma bands (Fig. 5). The increased nodal shortest path length of a node indicated larger separations between it and other nodes in the network, suggesting that the costs for information transmission and integration were expensive in mAD compared with aMCI.

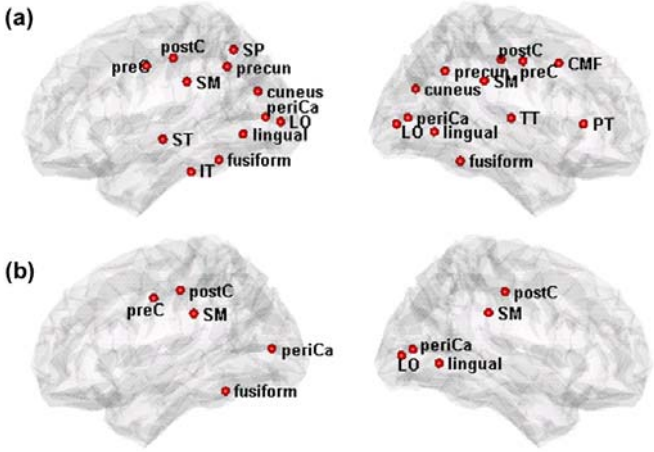


Fig. 5 The cortical regions with significant increases in nodal shortest path length for mAD compared with aMCI in the (a) beta2 and (b) gamma bands. The plots are displayed from left (left column) and right (right column) lateral views

In the results of nodal efficiency, significant alterations between mAD and aMCI groups were observed in different cortical regions in the delta, theta, beta2, and gamma bands (Fig. 6). In the low-frequency delta band, regions with significantly reduced nodal efficiency in mAD mainly distributed in the right hemisphere, covering right inferior frontal (POP, PT, and PO), temporal (paraH, insula, ST, TT, and EC), parietal, and

occipital regions. The delta waves of EEG have been reported to be characterized by right lateralization focused on the thalamus-connected frontal, parietal and temporal cortices [35]. The distributed regions with significantly decreased nodal efficiency lateralized to the right hemisphere in the delta band may reflect the disrupted connections between the thalamus and multiple cortical regions. In the high-frequency beta2 band, regions with significantly reduced nodal efficiency in mAD mainly located in bilateral parietal, temporal, occipital regions, and right frontal regions. Two limbic regions (PC and IC) also exhibited significant reduction of nodal efficiency in the beta2 band for mAD.

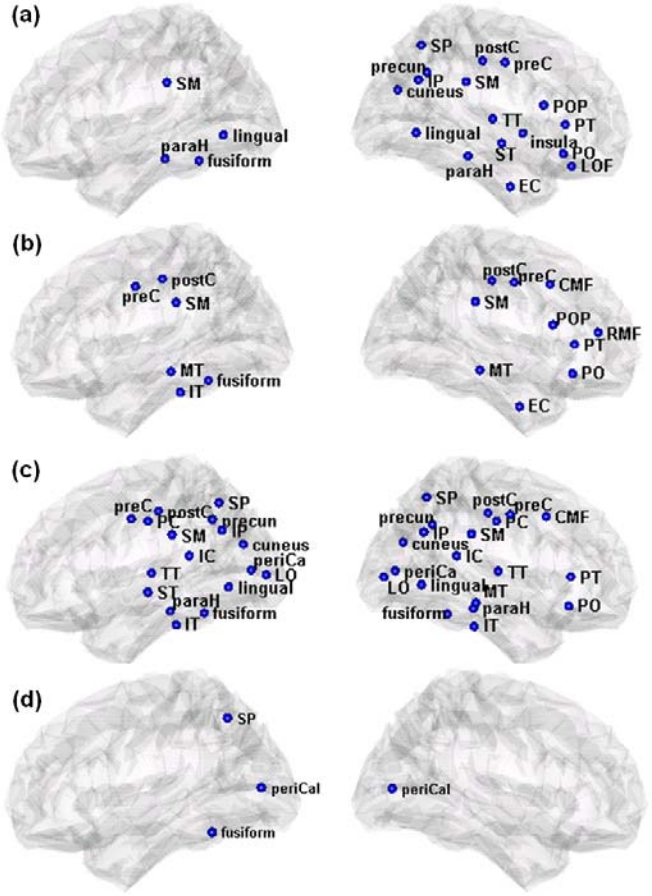


Fig. 6 The cortical regions with significant decreases in nodal efficiency for mAD compared with aMCI in the (a) delta, (b) theta, (c) beta2, and (d) gamma bands. The plots are displayed from left (left column) and right (right column) lateral views

IV. Conclusion

A question central to this study is whether mAD exhibited alterations in functional network organization compared with aMCI. In the comparison of the topology of resting-state cortical networks between two groups, the disruptions of network integrity and reductions of network efficiency in mAD characterized by lower degree, decreased clustering coefficient, higher shortest path length, and reduced global and local efficiencies in the delta, theta, beta2, and gamma bands are evident.

Open Science Index, Biomedical and Biological Engineering Vol:8, No:11, 2014 publications.waset.org/9999740/pdf

Acknowledgment

The study was funded in part by the National Science Council (NSC100-2314-B-010-022-MY2, NSC102-2221-E-010-013-MY3, NSC102-2314-B-010-059), the Taipei City Hospital (102TPECH10), the National Science Council supported for the Center for Dynamical Biomarkers and Translational Medicine, National Central University, Taiwan (NSC 101-2911-I-008-001) and Brain Research Center, National Yang-Ming University and a grant from Ministry of Education, Aim for the Top University Plan.

References

[1] R. C. Petersen, "Early diagnosis of Alzheimer's disease: is MCI too late?," *Current Alzheimer Research*, vol. 6, p. 324, 2009.

[2] A. Pozueta, E. Rodríguez-Rodríguez, J. L. Vazquez-Higuera, I. Mateo, P. Sánchez-Juan, S. González-Perez, J. Berciano, and O. Combarros, "Detection of early Alzheimer's disease in MCI patients by the combination of MMSE and an episodic memory test," *BMC neurology*, vol. 11, p. 78, 2011.

[3] S. Landau, D. Harvey, C. Madison, E. Reiman, N. Foster, P. Aisen, R. Petersen, L. Shaw, J. Trojanowski, and C. Jack, "Comparing predictors of conversion and decline in mild cognitive impairment," *Neurology*, vol. 75, pp. 230-238, 2010.

[4] X. Delbeuck, M. Van der Linden, and F. Collette, "Alzheimer'disease as a disconnection syndrome?," *Neuropsychology review*, vol. 13, pp. 79-92, 2003.

[5] M. Bozzali, G. J. Parker, L. Serra, K. Embleton, T. Gili, R. Perri, C. Caltagirone, and M. Cercignani, "Anatomical connectivity mapping: a new tool to assess brain disconnection in Alzheimer's disease," *Neuroimage*, vol. 54, pp. 2045-2051, 2011.

[6] D. Popivanov, J. Dushanova, "Non-linear EEG dynamic changes and their probable relation to voluntary movement organization," *Neuroreport*, vol. 10, pp. 1397–401, 1999.

[7] C. Andrew, G. Pfurtscheller, "Lack of bilateral coherence of post-movement central beta oscillations in the human electroencephalogram," *Neurosci. Lett.*, vol. 273, pp. 89–92, 1999.

[8] P.L. Nunez, R. Srinivasan, A.F. Westdorp, R.S. Wijesinghe, D.M. Tucker, R.B. Silberstein et al., "EEG coherency: I: statistics, reference electrode, volume conduction, Laplacians, cortical imaging, and interpretation at multiple scales," *Electroencephalogr. Clin. Neurophysiol.*, vol. 103, pp. 499–515, 1997.

[9] C.F. Lu, S. Teng, C.I. Hung, P.J. Tseng, L.T. Lin, P.L. Lee, Y.T. Wu, "Reorganization of functional connectivity during the motor task using EEG time–frequency cross mutual information analysis," *Clinical Neurophysiology*, vol. 122, no. 8, pp. 1569-1579, 2011.

[10] C. Shannon, "A mathematical theory of communication," *Bell Syst Tech J*, vol. 27, pp. 379–426, 1948.

[11] Y. Liu, C. Yu, X. Zhang, J. Liu, Y. Duan, A. F. Alexander-Bloch, B. Liu, T. Jiang, and E. Bullmore, "Impaired long distance functional connectivity and weighted network architecture in Alzheimer's disease," Cerebral Cortex, vol. 24, pp. 1422-1435, 2014.

[12] C. Stam, B. Jones, G. Nolte, M. Breakspear, and P. Scheltens, "Small-world networks and functional connectivity in Alzheimer's disease," Cerebral Cortex, vol. 17, pp. 92-99, 2007.

[13] M.F. Folstein, S.E. Folstein, P.R. McHugh, "Mini-mental state. A practical method for grading the cognitive state of patients for the clinician," *J. Psychiatr. Res.*, vol. 12, pp. 189–198, 1975.

[14] J.C. Morris, "The Clinical Dementia Rating (CDR): current version and scoring rules," *Neurology*, vol. 43, pp. 2412–2414, 1993.

[15] R.C. Petersen, "Mild cognitive impairment as a diagnostic entity," *J. Intern. Med.*, vol. 256, pp. 183–194, 2004.

[16] G. McKhann, D. Drachman, M. Folstein, R. Katzman, D. Price et al,. "Clinical diagnosis of Alzheimer's disease: report of the NINCDS-ADRDA Work Group under the auspices of Department of Health and Human Services Task Force on Alzheimer's Disease," *Neurology*, vol. 34, pp. 939–944, 1984.

[17] A. Delorme, S. Makeig, "EEGLAB: an open source toolbox for analysis of single-trial EEG dynamics including independent component analysis." *J. Neurosci. Methods.*, vol. 134, pp. 9–21, 2004.

[18] A. Gramfort, T. Papadopoulo, E. Olivi, M. Clerc, "OpenMEEG: opensource software for quasistatic bioelectromagnetics," *BioMedical Engineering OnLine*, vol. 9, no. 1, pp.45, 2010.
[19] M.S. Hamalainen, R.J. Ilmoniemi, "Interpreting magnetic fields of the brain: minimum norm estimates," *Med. Biol. Eng. Comput.*, vol. 32, pp. 35–42, 1994.
[20] F.H. Lin, T. Witzel, S.P. Ahlfors, S.M. Stufflebeam, J.W. Belliveau et al, "Assessing and improving the spatial accuracy in MEG source localization by depth-weighted minimum-norm estimates," *Neuroimage*, vol. 31, pp. 160–171, 2006.
[21] F. Tadel, S. Baillet, J.C. Mosher, D. Pantazis, R.M. Leahy, "Brainstorm: a user-friendly application for MEG/EEG analysis," *Comput. Intell. Neurosci.*, 879716, 2011..
[22] D.L. Collins, A.P. Zijdenbos, V. Kollokian et al., "Design and construction of a realistic digital brain phantom," *IEEE Transactions on Medical Imaging*, vol. 17, no. 3, pp. 463–468, 1998.
[23] A. Klein, J. Tourville, "101 labeled brain images and a consistent human cortical labeling protocol," *Frontiers in neuroscience*, vol. 6, article 171, 2012.
[24] C.C. Chen, J.C. Hsieh, Y.Z. Wu, P.L. Lee, S.S. Chen, D.M. Niddam, T.C. Yeh, Y.T. Wu, "Mutual-information-based approach for neural connectivity during self-paced finger lifting task," *Human brain mapping*, vol. 29, no. 3, pp. 265-280, 2008.
[25] M. Rubinov, O. Sporns, "Complex network measures of brain connectivity: Uses and interpretations," *Neuroimage*, vol. 52, pp. 1059–1069, 2010.
[26] M.D. Humphries, K. Gurney, "Network 'Small-world-ness': a quantitative method for determining canonical network equivalence," *PLoS One*, vol. 3, article e0002051, 2008.
[27] V. Latora, M. Marchiori, "Efficient behavior of small-world networks," *Phys. Rev. Lett.*, vol. 87, article 198701, 2001.
[28] E. Bullmore, O. Sporns, "Complex brain networks: graph theoretical analysis of structural and functional systems," *Nat. Rev. Neurosci.*, vol. 10, pp. 186–198, 2009.
[29] S. Achard, E. Bullmore, "Efficiency and cost of economical brain functional networks," *PLoS Comput. Biol.*, vol. 3, no. 2, article e17, 2007.
[30] Y. Benjamini, Y. Hochberg, "Controlling the false discovery rate: a practical and powerful approach to multiple testing," *J. R. Stat. Soc. Series B Stat. Methodol.*, vol. 57, pp. 289–300, 1995.
[31] Y. He, Z. Chen, G. Gong, A. Evans, "Neuronal Networks in Alzheimer's Disease," *Neuroscientist*, vol. 15, pp. 333-350, 2009.
[32] Y. Liu, C. Yu, X. Zhang, J. Liu, Y. Duan, A.F. Alexander-Bloch, B. Liu, T. Jiang, E. Bullmore, "Impaired long distance functional connectivity and weighted network architecture in Alzheimer's disease," *Cerebral Cortex*, vol. 24, no. 6, pp.1422-1435, 2014.
[33] R.P. Vertes, "Hippocampal theta rhythm: a tag for short-term memory," *Hippocampus*, vol. 15, no. 7, pp. 923–935, 2005.
[34] Y. Kubota, W. Sato, M. Toichi, T. Murai, T. Okada, A. Hayashi, A. Sengoku, "Frontal midline theta rhythm is correlated with cardiac autonomic activities during the performance of an attention demanding meditation procedure," *Cognitive Brain Research*, vol. 11, no. 2, pp. 281-287, 2001.
[35] R.E. Mistlberger, B.M. Bergmann, A. Rechtschaffen, "Relationships among wake episode lengths, contiguous sleep episode lengths, and electroencephalographic delta waves in rats with suprachiasmatic nuclei lesions," *Sleep*, vol. 10, no. 1, pp. 12-24, 1987.

Open Science Index, Biomedical and Biological Engineering Vol:8, No:11, 2014 publications.waset.org/9999740/pdf